LAWRENCE
LIVERMORE
NATIONAL
LABORATORY

LLNL-TR-420285

The development of the time dependence of the nuclear EMP electric field

C. Eng

November 16, 2009

Disclaimer

This work performed under the auspices of the U.S. Department of Energy by Lawrence Livermore National Laboratory under Contract DE-AC52-07NA27344.

The development of the time dependence of the nuclear EMP electric field

Chester D. Eng

***Abstract*— The nuclear electromagnetic pulse (EMP) electric field calculated with the legacy code CHAP is compared with the field given by an integral solution of Maxwell's equations, also known as the Jefimenko equation, to aid our current understanding on the factors that affect the time dependence of the EMP. For a fair comparison the CHAP current density is used as a source in the Jefimenko equation. At first, the comparison is simplified by neglecting the conduction current and replacing the standard atmosphere with a constant density air slab. The simplicity of the resultant current density aids in determining the factors that affect the rise, peak and tail of the EMP electric field versus time. The three dimensional nature of the radiating source, i.e. sources off the line-of-sight, and the time dependence of the derivative of the current density with respect to time are found to play significant roles in shaping the EMP electric field time dependence. These results are found to hold even when the conduction current and the standard atmosphere are properly accounted for. Comparison of the CHAP electric field with the Jefimenko electric field offers a direct validation of the high-frequency/outgoing wave approximation.**

***Index Terms*—EMP radiation effects, nuclear explosions, Maxwell equations, radiation sources.**

I. INTRODUCTION

Nuclear electromagnetic pulse (EMP) theory was developed over forty years ago by Longmire [1]-[5] and Karzas and Latter [6]. Their theory describes the physics of EMP generation and predicts the magnitude and time dependence of the electric and magnetic fields. Essentially, gamma rays from a nuclear burst interact with the atmosphere between the altitudes of 20 and 40 km (i.e. the EMP source region) to produce Compton electrons with kinetic energies of approximately 1 MeV. These energetic electrons are then accelerated in the earth's magnetic field resulting in a transverse source current perpendicular to the path of the original gamma ray. Compton ionization of the air also generates the secondary electrons for a return current. The combination of the source and the return current produces an electromagnetic pulse with amplitude no larger than a few tens of kilovolts per meter due to saturation [2]. The amplitude of the pulse propagating away from the burst point can be quite large compared to the pulse propagating back toward the burst point because the *apparent* movement of the source trails the EMP. This motivated Longmire to use the "outgoing" wave approximation or, equivalently, Karzas and Latter to use the "high frequency" approximation in their formulation.

The physics of EMP theory is widely accepted because of its ability to explain the peak electric fields and the time dependence of the EMP. However, proper experimental verification of the theory has never been borne out to due to the end of high-altitude nuclear testing in 1962. Several EMP researchers have instead opted to validate the theory analytically. In [5], Longmire considered the EMP from a uniform planar source of radiating electrons. The electrons in the source begin radiating at the same moment in time so as to simulate a planar pulse of gamma rays normally incident on a planar layer of air molecules. Although this set-up is somewhat artificial, Longmire was able to rederive the same one-dimensional planar wave equation under the outgoing/high-frequency approximation after properly accounting for the path-length time delay of the signals from each electron in the planar source. This demonstrated that the wave equation first derived by Longmire does account for a spatially distributed source as long as the outgoing wave approximation was satisfied. Radasky *et al*. [7] used a similar approach and rederived the EMP wave equation utilizing the high frequency approximation. In the derivation process [7] correctly shows that the EMP electric field is proportional to the radial integral of the current density evaluated at the appropriate retarded time and along the line-of-sight[1] between the nuclear explosion and the observer. The significance of this result is that the characteristics of the source along the LOS are important in determining the properties of the EMP at the observer[2]. In both of the above reports, the authors performed these calculations to validate the formulation of the equations used in numerical calculations.

Recently, Roussel-Dupré [8] examined the EMP produced by the prompt radiation from a nuclear explosion using two different approaches. One is based on a particle approach that starts with the Liénard-Wiechert potentials. In this case the synchrotron radiation generated by individual Compton electrons turning in an external or self-consistent magnetic

The author is with the Lawrence Livermore National Laboratory, Livermore, CA 94551 USA (e-mail: ceng@ llnl.gov).

[1] Hereafter, line-of-sight will be abbreviated as LOS.

[2] The reader should not confuse the radial integral (a product of the original *volume* integral) of the current evaluated along the LOS in [7] as a line integral. That is, the radial integral does not imply that the EMP is due only to sources emitted only along the LOS.

field is summed coherently over the source region to yield an expression for the radiated electric field at the observer. The other approach adopts the high-frequency approximation and a fluid treatment for the electrons. In this case [8] is able to derive an expression for the EMP at the observer that is equivalent to previous work based on a solution of Maxwell's equations (cf. [1]-[6]). In the end, [8] demonstrates that these two very different approaches yield identical results under the same approximations[3].

The approach in this paper will be to compare the results of the electric field versus time given by a legacy EMP code called CHAP [4] with the field from the Jefimenko integral solution (1) of Maxwell's equations [9], [10]. Note that the Jefimenko solution is exact and does not use the high-frequency approximation. We consider a nuclear explosion at an altitude of 100 km and calculate the EMP electric field at an observer on the ground directly below. To make the comparison between CHAP and the integral solution meaningful the current density required for the integral solution is extracted from the CHAP calculation.

Solving the Jefimenko integral numerically provides several advantages over the analytical methods used by others. First, the volume of integration is easily modified so the effects of the spatial distribution of the source region could be studied very easily. Certain regions of the source region can be easily blocked off from the calculation. Second, the current source used in CHAP could be used in the integral solution to provide a meaningful comparison of the two calculations. The current source from CHAP is not a simple function and therefore cannot be integrated easily using analytical methods. Any modifications to the CHAP calculation, such as the air density or conduction current, are easily carried over to the integral solution via the current density. Third, the numerical method is very simple to understand and implement. It does not require using the high-frequency/outgoing wave approximation. This makes the results of the integral calculation easier to understand while providing a straightforward method for validating the high-frequency/outgoing wave approximation used in CHAP. Finally, the Jefimenko equation is an integral of the radiation from point-like source elements of volume *dV*. For some, this particle approach is physically more intuitive than the continuum approach such as the one used by Longmire [1]-[5] because the EMP pulse can be visualized as the superposition of electromagnetic waves from point-like sources which depend on the *time-derivative* of the current density. In previous work, the current density is used as a source for the EMP and is given by a complicated integral over retarded time [6], [8].

Several simplifications to CHAP are implemented to help determine which factors control the time dependence of the EMP. The first simplification is to substitute the standard atmosphere in CHAP with a constant air density *slab* with $\rho_{\text{air}} = 5\times10^{-5}$ g/cm^3 between the altitudes of 20 and 30 km and zero everywhere else. The word slab is italicized because in CHAP spherical coordinates are used instead of Cartesian coordinates so the slab is really a section of a thick spherical shell. The second simplification is to reduce the effects of the conduction current density to a negligible level compared to the Compton electron current density. These two simplifying modifications lead to a source current density that has the same time dependence throughout the slab. A single function for the current density is then used in the Jefimenko equation and the resultant electric field is then normalized so that its peak value is equal to one. The CHAP electric field is also similarly normalized. The electric fields from both calculations are then compared to determine any differences in their behavior with respect to time.

In a second calculation, the electric fields are calculated with the simplifications mentioned in the previous paragraph removed. The standard atmosphere is used and the conduction current is included. This time the un-normalized electric fields are compared to determine. This case is referred to as the standard case while the calculation with the simplifications is referred to as the simplified case.

The electric field due to sources only along the LOS is also calculated in both cases. To calculate this field the Jefimenko equation (1) is used again but the volume integration is limited to elements strictly along the LOS. Then comparing the CHAP, Jefimenko, and LOS electric fields we can show the importance of the sources lying off LOS in the time-development of the EMP.

The goal in all of these field comparisons is to understand intuitively what factors are important in shaping the time-dependence of the EMP electric field. Specific characteristics discussed here are the rise-time, which is defined as the time required for the electric field to change from 10% to 90% of the peak value of the electric field, the time of the peak, and the tail. Calculations that use a thin shelled source region and a modified current density are also presented to support this goal. As will be seen later on, the electrical field comparison will provide a strong confirmation of the high-frequency/outgoing wave approximation.

II. Calculating EMP with the Jefimenko Equation

The electric field $\mathbf{E}(\mathbf{r}',t)$ at some point $\mathbf{r}'$ and at time t is given by the equation

$$\mathbf{E}(\mathbf{r}',t) = \frac{1}{4\pi\varepsilon_0}\int_{source}\left[\frac{\rho(\mathbf{r},t_r)}{R^2}\hat{\mathbf{R}} + \frac{\dot{\rho}(\mathbf{r},t_r)}{cR}\hat{\mathbf{R}} - \frac{\dot{\mathbf{J}}(\mathbf{r},t_r)}{c^2R}\right]dV \tag{1}$$

where $\mathbf{r}$ is the position of a source element of volume dV,

[3] In [8], the use of the word coherent is not meant to imply that the EMP field is due to point-like sources along the line of sight. Instead, the radiation from point sources that make up the source region is coherent if the emission occurred before collisions disrupted the orbit of the Compton electron [12].

$R = |\mathbf{r} - \mathbf{r}'|$ is the distance between the source element and the point of observation, the origin of $\mathbf{r}'$ and $\mathbf{r}$ is the burst point in this case, $t_r = t - R/c$ is the retarded time, $\rho(\mathbf{r}, t_r)$ is the charge density and $\mathbf{J}(\mathbf{r}, t_r)$ is the current density. The dot above the source terms in the second and third terms in (1) indicate a derivative taken with respect to time t. Equation (1) is the Jefimenko integral solution to Maxwell's equations. If the current component is perpendicular to the LOS then the third term in (1) yields electromagnetic radiation since the other terms give a vector component along the $\hat{\mathbf{R}}$ direction. Therefore, the first and second terms will be ignored and the third term in (1) will be referred to as the radiation term as long as the perpendicular component of $\dot{\mathbf{J}}(\mathbf{r}, t_r)$ is used. The following sections explain how to obtain $\dot{\mathbf{J}}(\mathbf{r}, t_r)$ from CHAP, describe the geometry of the source region, and outlines the used to numerically evaluate the third integrand in (1) at a retarded time.

III. The source term $\dot{\mathbf{J}}(\mathbf{r}, t_r)$ for the simplified case

The current density for (1) is taken from the CHAP calculation. The time variable in CHAP is not the same as the retarded time in (1) so a time-conversion is discussed first. Then the modifications, for the simplified case, that convert the standard atmosphere to a constant density air slab and neglect the conduction current are discussed. Some CHAP parameters common to the simplified and the standard case are the 100 km height of burst, vertical look angle, the dipole magnetic field strength, the 90 degree magnetic dip angle, and the mono-energetic 2 MeV gamma ray spectrum with the generic time dependence [11] shown in Fig. 3.

A. The CHAP current density

The CHAP current density is needed in (1) so that a meaningful comparison can be made between the electric field from the CHAP code and the Jefimenko equation. In CHAP, spherical coordinates are used and the burst point as the origin. The current density is calculated at several radii r along the LOS between the burst point and the observer. The CHAP code has been set up so that the only current component in CHAP that yields an EMP electric field is the current J_θ, where $\hat{\boldsymbol{\theta}}$ is perpendicular to the LOS. CHAP assumes that J_θ is independent of the azimuth θ and zenith ϕ because variations of these angles do not yield significant changes in the EMP electric field on the timescales of interest [4], [6]. Hence, the only explicit spatial coordinate dependence in the CHAP current density is the radius r so that

$$J_\theta = J_\theta(r, t_{\mathrm{CHAP}}), \tag{2}$$

where the time in CHAP is t_{CHAP}.

Note that (2) implies the CHAP current source has a spherical distribution despite being calculated only along the LOS. For example, the radius of the sphere is $r \approx 75$ km for a burst point of 100 km altitude and a source region between 20 and 30 km. However, it will be shown later that only part of the spherical current distribution contributes to the EMP electric field within the first microsecond.

B. The relationship between t_{CHAP} and t_{r}

The relationship between the time t_{CHAP} and t_r is now given. In CHAP, the zero time, $t_{\mathrm{CHAP}} = 0$, corresponds to the moment that the gamma pulse arrives at a radiating source element irrespective of their position in *r*. This choice of reference point in time is convenient because it allows the superposition of signals generated at other radial points and also gives the time dependence of the EMP signal as seen by an observer on the ground where $t_{\mathrm{CHAP}} = 0$ also corresponds to the instant the ground observer begins recording the EMP. Therefore, choosing $t = 0$ to correspond with the time of the burst, the retarded time $t_r = t - R/c$ can be calculated as a function of t_{CHAP}, the radius r of the source element and the distance R between the source element and the ground observer with the equation

$$t_r = t_{\mathrm{CHAP}} + \frac{r+R}{c} - \frac{R}{c} \tag{3}$$

or simply,

$$t_r = t_{\mathrm{CHAP}} + \frac{r}{c}. \tag{4}$$

The time r/c in (3) is the time it takes the gamma pulse to reach the source element *dV* and *R/c* is the time it takes the electromagnetic signal from *dV* to reach the ground observer. Equation (4) can now be used to transform data from a function of t_{CHAP} to a function of t_r.

Note that from the definition of the retarded time a signal from a particular source element radiated at time t_{CHAP} after the arrival of the gamma pulse will reach the observer at time

$$t = t_{\mathrm{CHAP}} + \frac{r+R}{c} \tag{5}$$

where $(r+R)/c$ is the time it takes the gamma pulse to travel from the burst point to a source element plus the time it takes the EMP to travel from the source element to the observer.

C. Simplifying the current density

Modifications to CHAP that simplify the current density will now be described. These modifications are meant to

simplify the application of (1) by first separating the explicit dependence on r in $J_\theta(r,t_{\rm CHAP})$ so that $J_\theta(r,t_{\rm CHAP})=\eta(r)J_\theta(t_{\rm CHAP})$. It will then be argued in the next section that the function $\eta(r)$ can be set equal to one without affecting what is being studied which is the time dependence of the EMP. Although these modifications are not necessary, removing the explicit r dependence so that $J_\theta = J_\theta(t_{\rm CHAP})$ makes understanding the time dependence of the EMP much easier.

The first step to removing the explicit radial dependence from the current density is to neglect the conduction current. Normally, the current density in CHAP is a combination of the Compton current and the electron conduction current. The conduction current is made up of air molecule electrons that have been ejected by the energetic Compton electrons. A single Compton electron contributes approximately 10^5 electrons to form part of a plasma which the EMP must propagate through. The electric field of the EMP can accelerate these electrons to generate a conduction current that opposes the Compton current from continuously building up the EMP. At small radii, the EMP electric field is small so the conduction current is also small. At larger radii, however, the EMP electric field grows until the feedback from the conduction current limits the growth of the peak electric field. Therefore, by arbitrarily reducing the conduction current in CHAP to a value negligible compared to the Compton current the radial dependence due to the conduction current is also removed.

The second modification to CHAP that will allow the separation of variables is to set the air density in the source region from 20 to 30 km to a constant value of $\rho_{\rm air}=5\times10^{-5}$ cm^{-3} and to zero everywhere else. Then only the source region is dense enough to interact with the gamma rays and manifest a Compton electron current[4]. The constant density source region forces J_θ in CHAP to have practically the same time dependence at all radii. Therefore, the current density can then be written as

$$J_\theta(r,t_{\rm CHAP})=\eta(r)J_\theta(t_{\rm CHAP}). \tag{6}$$

Note that the factor $\eta(r)$ in (6) is proportional to the density of Compton electrons deposited at the radius r.

Fig. 2 shows the CHAP current density $J_\theta(t_{\rm CHAP})$ taken at a radius that corresponds to one-fifth of a 2 MeV gamma mean-free-path in our constant density slab shaped atmosphere. The peak of the current density in Fig. 2 has been normalized to one because only the time dependence is of interest and because the normalization makes it easier to compare the time dependence of similarly normalized variables. Note again that the current density in CHAP $J_\theta(t_{\rm CHAP})$ can be related to $J_\theta(t_r)$ by the use of (4).

[4] The mean-free-path of a 2 MeV gamma-ray photon in this source region is 4.5 km.

D. The time-derivative of the current density

As a result of (6), the time-derivative of the current density is given by

$$\dot J_\theta(r,t_{\rm CHAP})=\eta(r)\dot J_\theta(t_{\rm CHAP}). \tag{7}$$

Equation (7) together with (4) then gives

$$\dot J_\theta(r,t_r)=\eta(r)\dot J_\theta(t_r). \tag{8}$$

Note that the factor $\dot J_\theta(t_r)$ can be normalized so that its peak value equals one provided $\eta(r)$ is adjusted appropriately. Hereafter, the $\dot J_\theta(t_r)$ used in the simplified case is assumed to be normalized in this fashion.

Removing the r dependence by setting $\eta(r)=1$ in (8) is desirable because it simplifies the calculation of (1). To test whether this is possible we set $\eta=1$ for all r and found no change in the time-dependence of E_θ. Moreover, various functions for $\eta(r)$ have been tried but the time-dependence of the electric field remained the same and only the amplitude of the electric field changed by a constant factor. More will be said later but basically this means that the time-dependence of E_θ is fully developed by signals from source elements within a thin spherical shell between r and $r+dr$. Each shell emits a combined signal $\Delta E_\theta^{\rm shell}$ with the same time-dependence. The superposition in retarded time of the electric field emitted by other shells produce an overall electric field E_θ with the same time-dependence as $\Delta E_\theta^{\rm shell}$. Therefore, since only the time-dependence is of interest and because all the electric fields are eventually renormalized so that the peak value is equal to one, the value of η is set to $\eta=1$ for all r. Equation (8) can now be written as

$$\dot J_\theta = \dot J_\theta(t_r). \tag{9}$$

Using (9) as the source for the radiation term in (1) then gives

$$E_\theta(\mathbf{r}',t)=-\frac{1}{4\pi\varepsilon_0}\int_{source}\frac{\dot J_\theta(t_r)}{c^2R}\,dV'. \tag{10}$$

The vector notation for ground observer position $\mathbf{r}'$ in $E_\theta(\mathbf{r}',t)$ is still retained in (10) since the parameters used to calculate the current density depend on the LOS between the observer and the burst.

In Fig. 3, a plot of $\dot J_\theta$ is given as a function of $t_{\rm CHAP}$ which

is used in calculations of the electric field E_θ for the simplified case provided (4) is used to give the appropriate retarded time. In Fig. 3, $\dot{J}_\theta$ has been renormalized so that its peak value is $\dot{J}_{\theta,\max}=1$. The value $\dot{J}_\theta=\dot{J}_{\theta,\max}$ occurs at time $t_{\rm CHAP}=17$ ns which nearly coincides with the peak of the normalized gamma flux $\dot{\gamma}(t_{\rm CHAP})$ from the burst which is also shown in Fig. 3. Fig. 3 shows that $\dot{J}_\theta$ and $\dot{\gamma}$ have approximately a rise-time of 5 nanoseconds. Here the rise-time is defined as the time a variable changes from 10% to 90% of its maximum value. The advantage of normalizing the variables may be seen in Fig. 3 which shows that the rise-times of $\dot{J}_\theta$ and $\dot{\gamma}$ are basically the same. This result is expected since the current density is only due to the Compton electrons.

To summarize, for the simplified case the conduction current in CHAP is artificially reduced to a negligible value and a constant air density slab for the atmosphere is used to simplify the physics to reduce (1) to (10). The time-derivative of the current density $\dot{J}_\theta(t_r)$ given in Fig. 3 is then used for all the radiating source elements in (10). Renormalizing all the electric fields so that the peak value equals one makes it simpler to compare their time-dependence. These modifications make the physics that affects the EMP time-dependence, especially the effect of a spatially distributed source, easier to understand. Furthermore, (10) is simple to evaluate numerically. These modifications are by no means necessary as will be shown later when the Jefimenko equation is used to recreate a CHAP solution without modifications to the conduction current of the air density.

IV. Evaluation of the Retarded Integral

To evaluate (10) numerically the arrival time of the radiation from a single source element to the observer is needed. A source element that is a distance r from the burst point will begin radiating once the gamma pulse reaches it at time r/c after the burst (see Fig. 4). The wavefront of the pulse from the source element will then reach an observer that is a distance R away from the source element in a time R/c. Thus the arrival time is $(r+R)/c$. An observer at a distance $L_{\rm obs}$ away from the burst will first receive an EMP signal after a time $L_{\rm obs}/c$ after the burst. It is convenient to reset the time of the burst to occur at standard time $t=-L_{\rm obs}/c$ so that the observer measures the arrival of the EMP electric field at $t_{\rm obs}=0$. The relationship between the standard time t and the observer time $t_{\rm obs}$ is therefore

$$t=t_{\rm obs}-\frac{L_{\rm obs}}{c}. \tag{11}$$

Note that the radiation from source elements lying along the LOS all have the same arrival time of $t_{\rm obs}=0$ since they all have $r+R=L_{\rm obs}$.

The retarded integral equation (10) can now be evaluated numerically to give the electric field $E_\theta(t_{\rm obs})$ at the observer. An array for $E_\theta(t_{\rm obs})$ is divided up into bins that correspond to a particular time $t_{\rm obs}$. The value in each bin is the cumulative electric field amplitude of signals from many source elements. The time step $\Delta t_{\rm obs}$ of the bins is small enough to resolve the radiated signal from a single source element. Therefore, the radiation from a single source element that arrives at the observer will fill the bins of $E_\theta(t_{\rm obs})$ from $t_{\rm obs}=(r+R)/c$ to $t_{\rm obs}=T_{\rm CHAP}+(r+R)/c$, where $T_{\rm CHAP}$ is the maximum value of $t_{\rm CHAP}$, by an amount corresponding to the amplitude of the signal at time $t_{\rm obs}$. The amplitude may be positive or negative. A sufficient number of bins are used to cover a range in time comparable to the pulse length $E_\theta(t_{\rm obs})$ given by CHAP.

V. The Volume of Integration

The geometrical relationship between the burst point, source region and the observer used in our calculations is shown in Fig. 4. Here, the distance between the burst point and the observer is $L_{\rm obs}=100$ km. Again, the line-of-sight is a vertical line that connects the burst point and the observer. For the simplified case, the source region has the shape of a spherical cap with an inner radius of $r_{\rm inner}=70$ km, outer radius of $r_{\rm outer}=80$ km measured from the burst point, a half-angle span of $\theta_{\max}=\pi/40$ measured around the burst point, and azimuthal symmetry.

For the standard case, the inner and outer radii are determined by CHAP: $r_{\rm inner}=40$ km and $r_{\rm outer}=82$ km. The maximum angle used for the integral in (1) is $\theta_{\max}=\pi/20$.

For both cases, the source region is divided into hoop shaped cells (source elements) with the dimensions Δr and $r\Delta\theta$ (see Fig. 4). Both dimensions are approximately the speed of light times a one-fifth of the time it takes $\dot{J}_\theta(t_{\rm CHAP})$ in Fig. 3 to rise from 10% to 90% of its peak value which is approximately 5 nanoseconds. These dimensions ensure that the emitted radiation from many neighboring cells can destructively or constructively interfere with each other. Cell partitions were not created along the azimuthal direction $\hat{\phi}$ because these cells would have the same arrival time due to axial symmetry.

VI. Causality Ellipsoid and Vector Addition of the Electric Fields

The rise and fall of the EMP electric field usually occurs within the first 10^{-6} s after the time the ground observer

begins receiving the EMP. The source elements that contribute to the EMP during this time are contained within a narrow ellipsoidal region with the burst point and the observer point at the foci (see [7] and Fig. 1). If the observer and burst point are a 100 km apart, the length of the major and minor axes of the ellipsoid are 100.3 km and 3.88 km, respectively. The distance d_S between the LOS and a source element lying on the ellipsoid's surface at a radius of 75 km from the burst point is

$$d_S = 3.36 \text{ km}. \tag{12}$$

The angle α between the LOS and the line from the observer to a cell on the ellipsoid's surface (see Fig. 1) can then be calculated. For the latter cell with $d_S = 3.36$ km the angle is $\alpha = 7.65$ degrees which gives

$$E_\perp = E_S \cos(\alpha) = 0.991 E_S \tag{13}$$

where E_S is the peak electric field amplitude from a source element and $E_\perp$ is the component of $\mathbf{E}_S$ perpendicular to the LOS between the burst and the observer. The difference between $\cos(\alpha) = 0.991$ and 1 is small enough that difference in the alignment of the $\dot{J}_\theta$ vector from element to element can be neglected when calculating EMP signals up to 10^{-6} s in duration. Therefore the same function for $\dot{J}_\theta$ is used for all the source elements in (10) regardless of their alignment differences.

As another example, consider the ellipsoid that corresponds to arrival times within the first 10^{-8} s. The source element lying on the ellipsoid's surface and at a radius of 75 km from the burst point has a d_S = 0.335 km and $\cos(\alpha) = 0.999$.

VII. Results and Discussion

The electric fields calculated using either the Jefimenko equation (10) or CHAP are now compared. Two cases are considered. The first set of comparisons will be for the simplifications to the CHAP calculation and the second set of comparisons will be for the standard case which accounts for the conduction current and the standard atmosphere. For convenience, the subscript θ is dropped from all the variable names from here on.

A. Comparison of the CHAP and Jefimenko electric fields for the simplified case

The CHAP electric field $E_{\text{CHAP}}(t_{\text{obs}})$ is now compared to the electric field $E_{\text{JEF}}(t_{\text{obs}})$ calculated with (10). To determine how the spatial distribution of the source region affects the rise-time of the EMP two different regions of integration are used in the calculation of the electric field $E_{\text{JEF}}(t_{\text{obs}})$. The first region is the same as that described in section V and we call the electric field from this source E_{JEF}. The second region is limited only to source elements lying on the LOS. The size of these elements is the same as those described in section V. Therefore this second source region is 10 km long and approximately 6 cm wide. The electric field calculated from this source is called E_{LOS}.

Displayed in Fig. 5 are the electric fields $E_{\text{CHAP}}(t_{\text{obs}})$, $E_{\text{JEF}}(t_{\text{obs}})$, and $E_{\text{LOS}}(t_{\text{obs}})$. Each the curve has been normalized so that the peak amplitude is equal to one. Comparing the electric field E_{LOS} with $\dot{J}_\theta$ from Fig. 3 shows that they both have the same time-dependence. This is because in (10) the signal from a source element is

$$dE = \frac{1}{4\pi\varepsilon_0}\frac{\dot{J}}{c^2 R} dV \tag{14}$$

and because the source elements along the LOS all have the same arrival time $(r+R)/c = L_{\text{obs}}/c$. Therefore E_{LOS} has the same time dependence as dE which in turn is directly proportional to $\dot{J}$. In contrast, the electric fields $E_{\text{JEF}}(t_{\text{obs}})$ and $E_{\text{CHAP}}(t_{\text{obs}})$ clearly have the same time-dependence despite their different calculation methods. Neither $E_{\text{JEF}}(t_{\text{obs}})$ or $E_{\text{CHAP}}(t_{\text{obs}})$ have the same time dependence as $E_{\text{LOS}}(t_{\text{obs}})$. The fact that the Jefimenko equation explicitly accounts for the three dimensional shape of the spherically symmetric current density source plus the fact that the electric fields $E_{\text{JEF}}(t_{\text{obs}})$ and $E_{\text{CHAP}}(t_{\text{obs}})$ have the same time-dependence implies that the CHAP method must also account for the signals from source elements off the LOS. As we have discussed in section VI these off-LOS contributions can come from source elements up to a distance $d_S = 0.335$ km from the LOS for times $t_{\text{obs}} \le 10^{-8}$ s. For arrival times between $10^{-8} \text{ s} < t_{\text{obs}} < 10^{-7}$ s the distance is between $0.335 \text{ km} < d_S < 1.06 \text{ km}$. Similarly, for arrival times between $10^{-7} \text{ s} < t_{\text{obs}} < 10^{-6}$ s the distance is between $1.06 \text{ km} < d_S < 3.36 \text{ km}$. How these signals superpose in time to form the rise-time, peak and the tail of the EMP is the subject of the next section. A simple example is worked out in the appendix.

B. The time dependence of E_{CHAP} in the simplified case

In Fig. 5, the rise-time of $E_{\text{CHAP}}(t_{\text{obs}})$ is approximately 8.4 ns. The peak of E_{CHAP} occurs at $t_{\text{obs}} = 24.4$ ns. After peaking, it takes approximately 179 ns for E_{CHAP} to decrease to 10% of the maximum value. On the other hand the rise-time of the signal dE_{JEF} from a single source element is 5 ns. After the

peak, the signal dE_{JEF} quickly drops to zero 25 ns after this signal began. According to the ground observer, the signals from source elements on the LOS arrive at the time $t_{\mathrm{obs}}=0$. A moment later, signals from just off the LOS arrive while signals on the LOS are still being transmitted to the observer. As more signals arrive the electric field E_{CHAP} continues to rise until $t_{\mathrm{obs}}=25$ ns. At this time, the observer "sees" the signal from source elements on the LOS change from a positive to a negative value and so the electric field E_{CHAP} peaks at this moment and begins to decrease. Note that the time of the crossover (i.e. $t_{\mathrm{obs}}=25$ ns) only determines when the peak occurs and not the magnitude of the EMP.

In Fig. 5, E_{CHAP} approaches zero as t_{obs} approaches $1\ \mu s$. At this time, the rate of positive valued signals reaching the observer nearly equals the rate of negative valued signals. This is a consequence of the integral of dE_{JEF} over all time being equal to zero or equivalently

$$\int_0^{\infty} \dot{J}\left(t_{\mathrm{CHAP}}\right)\mathrm{d}t_{\mathrm{CHAP}}=0. \tag{15}$$

To emphasize the importance of the negative value of $\dot{J}$ the electric field E_{JEF}^{+} is calculated with (10) using a source $\dot{J}^{+}$ that has $\dot{J}^{+}\geq 0$ at all t_{obs}. The source $\dot{J}^{+}$ is basically the same as $\dot{J}$ in Fig. 3 except the negative values of $\dot{J}$ are converted to zero. The result E_{JEF}^{+} is shown in Fig. 6 as a function of t_{obs}. Here, E_{JEF}^{+} develops a plateau rather than a peak. The plateau is due to the constant rate of positive valued signals reaching the observer. Eventually, E_{JEF}^{+} drops to zero at $t_{\mathrm{obs}}=10^{-6}$ s because there are not enough source elements in our problem that begin to radiate beyond this time. Therefore, without the negative part of $\dot{J}$ the EMP electric field develops into a long flat pulse instead of the tail found in the electric field E_{CHAP}.

C. The time dependence of $\mathrm{E_{JEF}}$ *due to a thin spherical shell source for the simplified case*

To explore the importance of the off-axis contributions to EMP even further, (10) is used to calculate the electric field $E_{\mathrm{thin}}\left(t_{\mathrm{obs}}\right)$ due to a thin shelled source with a radial thickness of $\Delta r=0.5$ m. The field E_{thin} is compared to the electric field $E_{\mathrm{thick}}\left(t_{\mathrm{obs}}\right)$ due to a thick shelled source region with a radial thickness of $\Delta r=10$ km. Both electric field calculations are made with the same $\dot{J}$ given in Fig. 3. Hence, $E_{\mathrm{thick}}\left(t_{\mathrm{obs}}\right)$ is the same as $E_{\mathrm{JEF}}\left(t_{\mathrm{obs}}\right)$ from Fig. 4. Fig. 7 shows the normalized electric fields $E_{\mathrm{thin}}\left(t_{\mathrm{obs}}\right)$ and $E_{\mathrm{thick}}\left(t_{\mathrm{obs}}\right)$ with exactly the same time dependence. This result holds no matter what thickness or radius is used for the thin shelled source.

Moreover, the time dependence of E_{thin} is the same as the current density J shown in Fig. 2. The proportionality between E_{thin} and J is predicted by the equation for the EMP electric field under the high-frequency approximation (equation (52) in [6]; equation (9) in [7] and equation (17) in [8]). When the secondary electrons are not included this equation is

$$E\left(\mathbf{r},\tau\right)=-\left(2\pi/cr\right)\int_0^{r} dr'r'J\left(\mathbf{r}',\tau\right). \tag{16}$$

For a thin shelled source (16) gives

$$\Delta E\left(\mathbf{r},\tau\right)=-\left(2\pi/cr\right)J\left(\mathbf{r}',\tau\right)r'\Delta r' \tag{17}$$

where r and r' are the radius of the observer and shell source from the burst point, respectively. Equating E_{thin} to ΔE in (17) therefore implies that the current density term on the right hand side of (17), which is evaluated along the LOS as shown by [7], accounts for all the point-like source elements, which emit an electric field proportional to $\dot{J}$, in the thin shell.

D. Comparison of the CHAP and Jefimenko electric fields for the standard case

In the standard CHAP simulation the standard atmospheric density is used and the effects of the conduction current are included. The conduction current consists of secondary electrons produced via the ionization of air molecules by Compton electrons. In the presence of an electric field the secondary electrons tend to short out the EMP electric field. This implies that the conduction current opposes the Compton current. However, the cancellation does not occur immediately because it requires time for the Compton electrons to lose most of their kinetic energy to ionization. The magnitude of the conduction current, J_{σ}, depends on the density of the secondary electrons and the strength of the EMP electric field and is given by the $J_{\sigma}=\sigma E$, where σ is the conductivity. Within the source region the air density is sufficiently high to make ionization via Compton electrons frequent enough that in a short time after $t_{\mathrm{CHAP}}=0$ the conduction current can become large enough to limit the growth of the electric field by the Compton current. The electric field is then said to be saturated and is given by $E_{\mathrm{peak}}=-J_C/\sigma$, where E_{peak} and J_C are the theta component of the EMP electric field and the Compton current, respectively [2].

For the integral solution approach (10) the source of the EMP electric field is the time derivative of the total current density which is given by

$$\dot{J}_{\mathrm{total}}=\dot{J}_C+\dot{J}_{\sigma}. \tag{18}$$

As before, the variables in (18) are the vector component perpendicular to the LOS. Since the standard atmosphere is used the source region is not the same as that defined in section V. Hence, the total current density is now a function of radius r as well as the retarded time t_r. To calculate the electric field $E_{\rm JEF}^{\rm total}$ the third term in (1) is used so that

$$E_{\rm JEF}^{\rm total}\left(\mathbf{r}',t\right) = -\frac{1}{4\pi\varepsilon_0}\int_{source}\frac{\dot{J}_{\rm total}\left(r,t_r\right)}{c^2 R}\,dV\,. \qquad (19)$$

The source $\dot{J}_{\rm total}\left(r,t_r\right)$ is given by the CHAP simulation. However, many radial points in the CHAP simulation are necessary to ensure that the total current changes slowly from point to point otherwise odd results occur in the application of (19). All parameters for the CHAP calculation are the same as the simplified case such as the height of burst, the magnetic field strength, the 2 MeV mono-energetic gamma ray spectrum and the vertical LOS.

The electric field $E_{\rm LOS}^{\rm total}$ due to just the LOS source elements is also calculated with (19) using the same source $\dot{J}_{\rm total}\left(r,t_r\right)$ obtained from the CHAP calculation.

As before, the normalized electric fields $E_{\rm CHAP}^{\rm total}$, $E_{\rm JEF}^{\rm total}$ and $E_{\rm LOS}^{\rm total}$ versus time are plotted in Fig. 8 but for the standard case. As in the case of the constant density air slab and zero conduction current, the electric field $E_{\rm JEF}^{\rm total}$ overlaps the field given by CHAP $E_{\rm CHAP}^{\rm total}$. The electric field $E_{\rm LOS}^{\rm total}$, however, is still unlike the CHAP solution $E_{\rm CHAP}^{\rm total}$ and demonstrates that the CHAP electric field is not a simple coherent superposition of signals emitted along the LOS even when the conduction current is included. Instead, the electric field given by CHAP must include emissions from a spatial distribution of sources that are not on the LOS in order to construct the time behavior of the EMP electric field from $t_{\rm obs} = 0$ to 10^{-6} s. Moreover, the ratio of the peak value of the non-normalized CHAP electric field (which is not shown but it is approximately 30 kV/m) to the non-normalized peak electric field calculated using (19) for the full source region is 0.983. In other words not only can (19) recreate the time-dependence of the CHAP EMP electric field but it can also duplicate the magnitude of the EMP electric field. Although the magnitude of the EMP electric field is determined by the strength of the Compton and conduction currents, the time of the peak is determined by a mechanism similar to that in the simplified case.

The construction of the time behavior of the EMP electric field $E_{\rm CHAP}^{\rm total}$ in the standard case, however, is more complicated than in the simplified case because here the source $\dot{J}_{\rm total}\left(r,t_r\right)$ does not have the same time-dependence at all radii r. However, the principles learned from that case apply here as well because the Jefimenko integral solution treats all current sources equally. Fig. 9 shows the EMP electric field using (19) but the region of integration is restricted to sources within an ellipsoid of causality of some size. As in section VI, the foci of the ellipsoids are the burst point and the ground observer. The *size* of the ellipsoids is indicated on Fig. 9 by a time next to each solid line curve. The time is given by $\left(r+R\right)/c$ where r is the distance from the burst point to any source element on the surface of the ellipsoid and R is the distance from that same source element to the ground observer. Basically, the larger times correspond to larger ellipsoids. For example, in section VI.A, we showed that $d_S = 0.335$ km for $\left(r+R\right)/c = 10^{-8}$ s and $d_S = 1.06$ km for $\left(r+R\right)/c = 10^{-7}$ s. Within the time interval $0 \le t_{\rm obs} \le \left(r+R\right)/c$ measured by the ground observer, the initial part of the signal from each source element within the $\left(r+R\right)/c$ ellipsoid should have reached the observer. However, the radiation from each element may still radiate out in time beyond $\left(r+R\right)/c$. The curve $E_{\rm CHAP}^{\rm total}$ is also included in Fig. 9 as a dashed line as a reference. All the curves in Fig. 9 have been normalized by the same number used to make the peak of $E_{\rm CHAP}^{\rm total}$ equal to one.

In Fig. 9, the electric field pulse from the region enclosed by the 10^{-9} s ellipsoid is small compared to $E_{\rm CHAP}^{\rm total}$. The total energy of the electric field pulse from the 10^{-9} s ellipsoid is only 0.3% of the total for $E_{\rm CHAP}^{\rm total}$. A source element on the 10^{-9} s ellipsoid that is at an altitude of 30 km is 113 m away from the LOS. For this ellipsoid the source elements are relatively close to the LOS so the electric field will more closely resemble the coherent superposition of signals along the LOS. A delay of 10^{-9} s does little to change the coherent superposition of the signals because the source $\dot{J}_{\rm total}\left(r,t_r\right)$ increases only to approximately 15% of its peak value 10^{-8} s after the arrival of a gamma pulse. Therefore, the time-dependence of the electric field given by the 10^{-9} s ellipsoid is approximately that of $E_{\rm LOS}^{\rm total}$, which is the weighted average of the sources $\dot{J}_{\rm total}\left(r,t_r\right)$ along the LOS in Fig. 8.

To obtain the initial rise and peak of $E_{\rm CHAP}^{\rm total}$ with (19) requires integrating over at least the source region within the 1.8×10^{-8} s ellipsoid because the peak of $E_{\rm CHAP}^{\rm total}$ occurs at $t_{\rm obs} = 1.8\times10^{-8}$ s. As in the simplified case, the peak of $E_{\rm CHAP}^{\rm total}$ occurs when the radiation from elements first reaching the observer begin to change sign due to the source $\dot{J}_{\rm total}\left(r,t_r\right)$ changing sign. The change in sign for the weighted average of $\dot{J}_{\rm total}\left(r,t_r\right)$ along the LOS (i.e. $E_{\rm LOS}^{\rm total}$) occurs at time $t_{\rm obs} = 1.8\times10^{-8}$ s when electric field for the 10^{-9} s ellipsoid crosses from positive to negative.

From Fig. 9, it seems that integrating (19) over the 1.8×10^{-8} s ellipsoid gives an electric field that matches $E_{\rm CHAP}^{\rm total}$ very well up to approximately 2.8×10^{-8} s or about 10^{-8} s after the peak. This is because the source $\dot{J}_{\rm total}(r,t_r)$ approximately zero until about 10^{-8} s after the gamma pulse reaches the source element. If the source $\dot{J}_{\rm total}(r,t_r)$ had changed sooner, then the apparent agreement would not have reached as far as $t_{\rm obs}=2.8\times10^{-8}$ s.

To recreate the tail of the EMP electric field sources further away from the LOS are need. Fig. 9 shows that integrating (19) over sources within the 5×10^{-8} s ellipsoid can recreate $E_{\rm CHAP}^{\rm total}$ up to time $t_{\rm obs}=5\times10^{-8}$ s very well. The signals from these source elements are obviously not in phase with the signals emitted along the LOS because of the length of the tail of $E_{\rm CHAP}^{\rm total}$ in comparison to the positive portion of $\dot{J}_{\rm total}(r,t_r)$. A source element on the 5×10^{-8} s ellipsoid that is also at an altitude of 30 km is 793 m away from the LOS.

Finally, in Fig. 9 (see also Fig. 10), a negative pulse develops at late times in the Jefimenko integral calculations. This pulse has an absolute amplitude and time-dependence similar to the early time positive pulse. In Fig. 5 and 8 the negative pulse is not shown on $E_{\rm JEF}$ or $E_{\rm JEF}^{\rm total}$ because the large ellipsoid of causality used in the calculations pushed the mirror pulse beyond a microsecond and outside the time range of the plot. Again, the simple example shown in the Appendix can explain how the negative pulse is built. Fig. 10 shows the negative pulse in curve *A* is given by the superposition of the negative portions of the late time sinusoids. Since all the sinusoids have the same constant amplitude, symmetry forces the positive and negative pulses on the curve *A* to have equal absolute magnitudes and the same time-dependence. In reality, however, the situation is not as simple as the example shown in Fig. 10. Several factors, such as the variation of the air density with altitude, distance from the observer, attenuation by secondary electrons, vector cancellation as discussed in section VI, can influence the contribution of the source elements as they move further away from the LOS. Measurements done during high-altitude nuclear test done in the past also do not reveal such a signal. To this author it seems more likely that the amplitude of the signals from sources very far away decreases with distance. In Fig. 11 one hundred single cycle sinusoids staggered in time are superposed but now their amplitudes vary as a function of time. The signals that arrive at late times correspond to signals from very far away and their amplitudes have been artificially reduced to reflect what might happen if the signals do decrease in strength as their distance from the LOS increases. As a result, Fig. 11 shows that at late times the amplitude of the sinusoids is so small that a negative pulse with amplitude comparable to the positive pulse cannot be produced.

E. Validity of the high-frequency or out-going wave approximations

The Jefimenko equation (1) is an exact solution of Maxwell's equations. In our numerical calculations of (10) or (19) the high-frequency/outgoing wave approximation is never used. The time-derivative of the current density is borrowed from CHAP but this quantity is not affected by the approximation. The CHAP formulation, however, utilizes the outgoing wave approximation in its calculation of the electric field. Therefore, the overlap of the electric fields by the two calculations shown in Figs. 5 and 8 is a strong validation of the high-frequency/outgoing wave approximation. A more detailed analysis can be done by calculating the value of χR as defined in [8] and then determining the path-length delay for a source element with this value.

The distance χR is approximately the distance from the LOS beyond which the Compton electrons no longer emit radiation that is coherent with those along the LOS and was used in [8] to calculate the volume of the source region that emitted radiation that reached the observer at the same time. The radius R is measured between the ground observer and the surface intersecting the source region that is radiating at the same retarded time. The angle χ is measured from the LOS and around the ground observer's position and is given by $\chi\approx\sqrt{2r'\Delta r/R^2}$. The radius r' is measured from the burst point to the radiating source and the maximum value of Δr is given by $\Delta r_{\rm max}=c(1-\beta)/\nu_E$ (from Fig. 1. of [8]). For a burst at 100 km altitude and a source region altitude of 25 km leads to the value of r = 75 km and R = 25 km. A value of $\Delta r_{\rm max}$ = 7.4 m for 1 MeV electrons at an altitude of 25 km is calculated from $\Delta r_{\rm max}$ = 0.24 m at sea level used in [8] by multiplying it by the ratio of the densities at sea level and at 25 km altitude. Consequently, the value of χR is 1.05 km. A source at this distance from the LOS would have an arrival time of 10^{-7} s. From Fig. 5 and 8 it is apparent that most if not all of the pulse is obtained before this time is reached. This justifies the volume of integration used in the analytical calculations of [8] for the EMP electric field under the particle approach which is the same as the equation obtained under the high-frequency approximation.

VIII. Concluding Remarks

In this paper, the EMP electric field is calculated from the Jefimenko integral which basically superposes the radiation from point-like source elements within a volume. These results indicate that the EMP electric field is not a simple superposition of signals from sources along the line-of-sight. Instead, the time dependence of the EMP electric field is built by contributions from sources off the line-of-sight whose signals do not reach the ground observer at the same time as those along the LOS due to path length differences. Sources at least 3.36 km away from the line-of-sight needed to be included in the Jefimenko equation to reproduce the CHAP EMP electric field up to a microsecond.

In the simplified case the signal from each source had the same time dependence as the time derivative of the current density $\dot{J}(t_r)$ which has a positive pulse initially followed by a negative pulse. It was shown that the rise-time of the EMP electric field is due to the superposition of the positive pulses from the sources. Eventually the first negative pulses reach the observer and at that point the EMP electric field reaches its peak value. The EMP electric field in the tail is the summation of negative and positive contributions from many current source elements rather than the slow decay of the source.

In the standard case, although the time-derivative of the current density $\dot{J}_{\text{total}}(r,t_r)$ is more complicated because of the explicit dependence on radius r, the build-up of time dependence of the electric field is qualitatively the same as that in the simplified case. Moreover, the principles developed in this paper are not limited to burst heights of 100 km and should apply to other physical conditions as well.

The electric field from the Jefimenko equation, which does not utilize the high-frequency or the outgoing wave approximation, was found to overlap the electric field calculated with CHAP. This implies that the high-frequency/outgoing wave approximation, which is used in the CHAP formulation, is valid.

APPENDIX

As a simple example to demonstrate the difference in rise-times between $E_{\text{JEF}}(t_{\text{obs}})$ and $E_{\text{LOS}}(t_{\text{obs}})$, we add the amplitudes from ten sinusoids each only one period T_{sin} long in time. Each sinusoid represents the radiation dE_{JEF} from a different source element arriving at the observer at different times. Thus the n-th sinusoid is added to the resultant beginning at time $\tau=(n-1)T_{\text{sin}}/10$. The resultant $A(\tau)$ is the sum of all the sinusoids and is meant to simulate $E_{\text{JEF}}(t_{\text{obs}})$. The sum of the sinusoids $A(\tau)$ is shown in Fig. 10 as a thick dashed line. This dashed line clearly has a time dependence different from each of the sinusoids just as $E_{\text{JEF}}(t_{\text{obs}})$ has a time dependence different from $dE_{\text{JEF}}(t_{\text{obs}})$. The curve $A(\tau)$ in Fig. 10 continues to rise until the negative amplitude from the first sinusoid begins cancelling the positive contributions from the $n>1$ sinusoids. Eventually, $A(\tau)=0$ when $\tau=90$ since there are equal contributions from positive and negative amplitudes. This is similar to what happens in Fig. 5 where the zero of $E_{\text{LOS}}(t_{\text{obs}})$ for the LOS elements occurs at the same time as the peak of $E_{\text{JEF}}(t_{\text{obs}})$. After $E_{\text{JEF}}(t_{\text{obs}})$ peaks it begins to decrease because of negative contributions radiated from some of the source elements arrive at the observer and cancel the positive contributions from other source elements.

In reality, a negative electric field pulse is not expected as in the curve $A(\tau)$. The signals from sources very far away have very late arrival times $(t_{\text{obs}} >> 10^{-6}\ s)$ and should therefore have little effect on the field at the observer due to air density variation with altitude, attenuation by secondary electrons, attenuation due to distance, and vector cancellation of the fields as discussed in section 6. Fig. 11 shows what happens when one hundred single cycle sinusoids staggered in time and with the amplitude $\tau\exp(-\tau/100)$ are added. As expected the late time negative pulse in the curve $A(\tau)$ disappears because the amplitude of the late time sinusoids goes to zero.

ACKNOWLEDGMENT

The author thanks David Simons, Hans Kruger, Robert Roussel-Dupré, Tom Thomson, Lynn Shaeffer, and Brian Yang for their helpful comments, guidance and encouragement.

REFERENCES

[1] C. L. Longmire, "Close In E. M. Effects Lectures X and XI", Los Alamos Scientific Lab, Los Alamos, NM, LAMS-3073, April 1964, unpublished.
[2] C. L. Longmire, IEEE Transactions on Electromagnetic Compatibility, vol. EMC-20, no. 1, p. 3, 1978.
[3] C. L. Longmire and H. J. Longley, "Improvements in the Treatment of Compton Current and Air Conductivity in EMP Problems", Defense Nuclear Agency, Report DNA-3192T, October 1971.
[4] H. J. Longley and C. L. Longmire, "Development of the CHAP EMP Code", Defense Nuclear Agency, Report DNA-3150T, January 1972, unpublished.
[5] C. L. Longmire, "Justification and Verification of High-Altitude EMP Theory – Part I", Lawrence Livermore National Laboratory, Livermore, CA, UCRL-15938, August 1987.
[6] W. J. Karzas and R. Latter, Phys. Rev. vol. 137, p. B1369, 1965.
[7] W. A. Radasky, W. J. Karzas, C. W. Jones and G. K. Schlegel, "High-Altitude Electromagnetic Pulse – Theory and Calculations", Metatech Corporation, Goleta, CA, DNA-TR-88-123, October 1988.
[8] R. A. Roussel-Dupré, IEEE Transactions on Electromagnetic Compatibility, vol. EMC-47, no.3, p.552, 2005.
[9] O. D. Jefimenko, Electricity and Magnetism, Electret Scientific, Star City, WV, 1989.
[10] J. D. Jackson, Classical Electrodynamics, Wiley, 1998, p. 246.
[11] S. Glasstone and P. J. Dolan, The Effects of Nuclear Weapons, United States Department of Defense and the United States Department of Energy, 3rd edition, 1977, p. 328.
[12] Private communication with R. A. Roussel-Dupré, 2009.

Chester D. Eng received the Ph.D. degree in physics from the University of Illinois at Urbana-Champaign in 2002.

For his graduate thesis he investigated the role of MHD waves in the early formation of stars via computer simulation. As a postdoctoral researcher (2002-2006) at Lawrence Livermore National Laboratory, Livermore, CA he examined the application of radar to lightning propagation and analyzed the physics of nuclear EMP generation. As a physicist at Lawrence Livermore National Laboratory (2006-present) he continued his work on EMP and also studied the effects of high-altitude nuclear explosions using computer simulations.

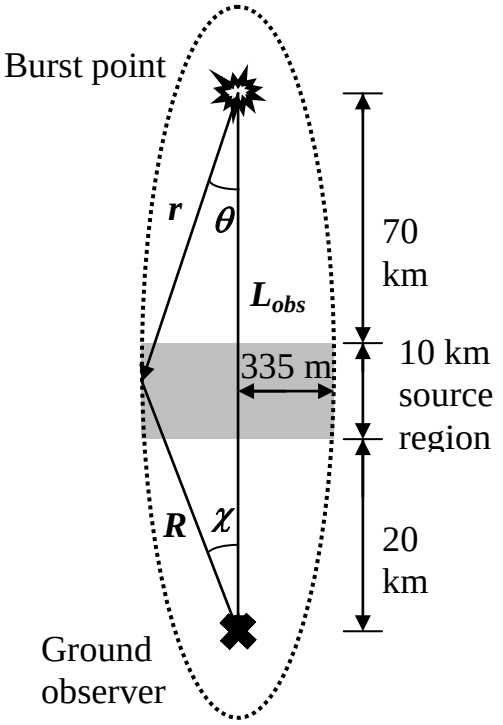

Fig. 1. Geometry of the constant density $\left(\rho_{\text{air}} = 5\times10^{-5}\ \text{g/cc}\right)$ source region with respect to the causality ellipsoid. The foci of the ellipsoid are the burst point and the observer. The ellipsoid is drawn such that $\left(r+R\right)/c = 10^{-8}\ \text{s}$. The distance from the line-of-sight of the point on the ellipsoid that is also at an altitude of 25 km is 335 m. The source region extends beyond the ellipsoid and lies between $r = 70\,\text{km}$ and $r = 80\,\text{km}$.

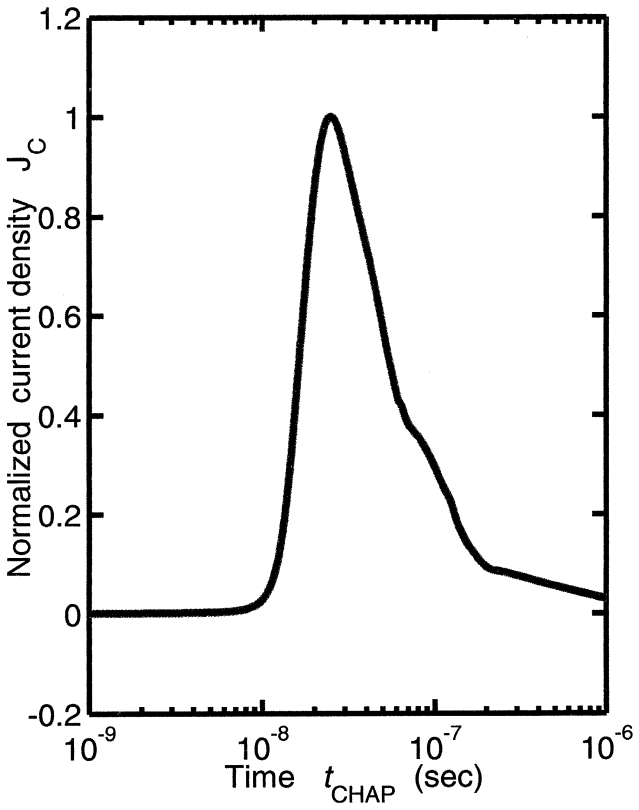

Fig. 2. A plot of the Compton current density J_C versus time t_{CHAP} given by the CHAP code for the case of constant density air slab and negligible conduction current.

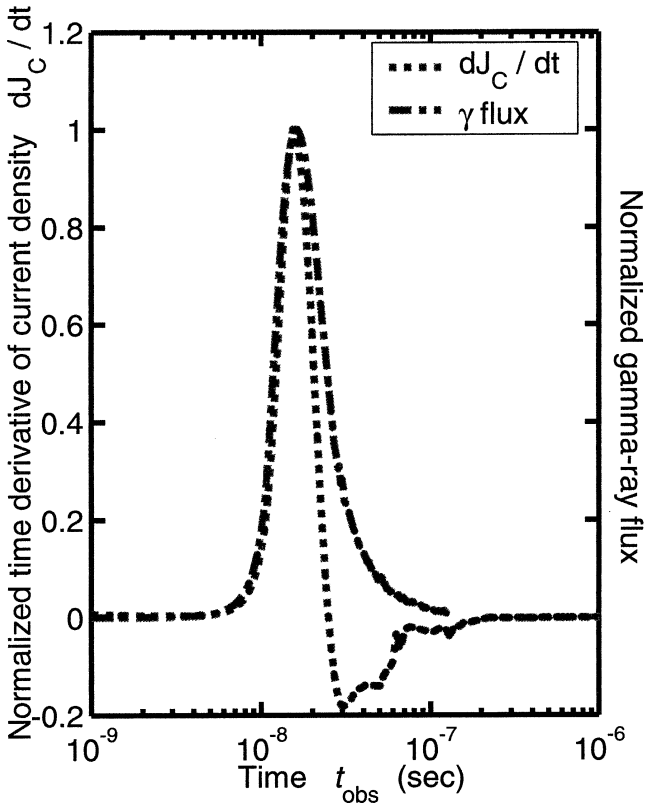

Fig. 3. The dotted line is a plot of the time derivative of the Compton current density $\dot{J}_C\left(t_{\mathrm{CHAP}}\right)$ versus t_{CHAP} for the case of constant density air slab and negligible conduction current. The dash-dot line is a plot of the gamma-ray flux versus t_{CHAP} used in the simplified and the standard cases. The time dependence of the gamma-ray flux is obtained from Glasstone and Dolan's book [11].

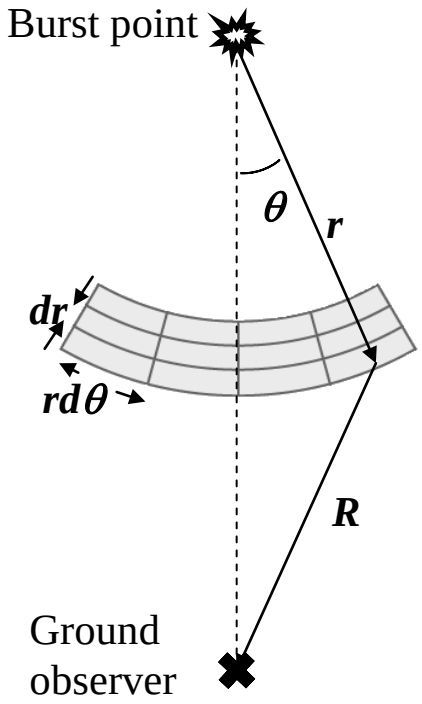

Fig. 4. The (r,θ) grid for the Jefimenko equation volume integration. The full region of integration is axially symmetric around the line-of-sight connecting the burst point and the ground observer. The volume of each hoop shaped cell is $dV = 2\pi r^2 \sin\theta\, d\theta\, dr$. For the simplified case, the region's inner radius is $r = 70\,\mathrm{km}$ and the outer radius is $r = 80\,\mathrm{km}$. The maximum angular position is $\theta_{\max} = \pi/100$. For the standard case, the radius of the region of integration is determined by the CHAP simulation. The maximum angular position in the standard case is $\theta_{\max} = \pi/40$.

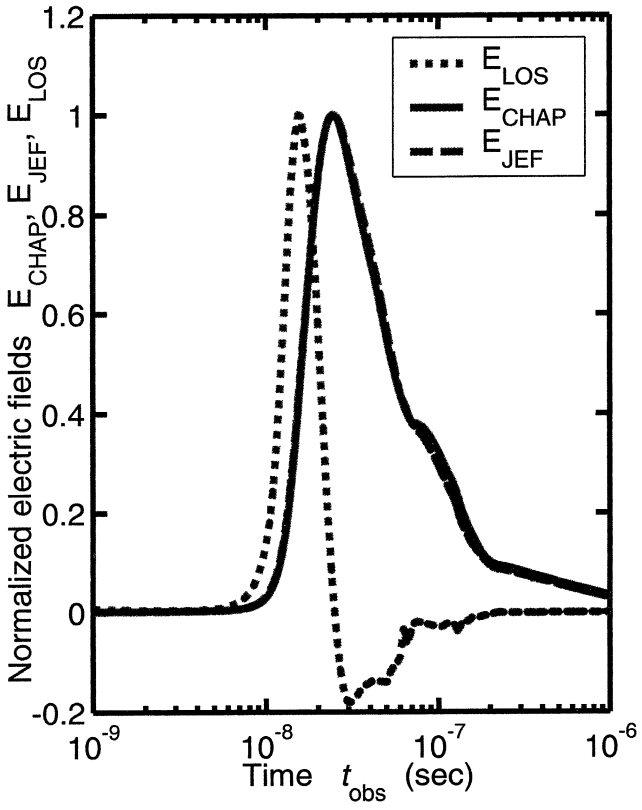

Fig. 5. Comparison of electric fields calculated with CHAP, E_{CHAP} (solid line), the Jefimenko equation, E_{JEF} (dashed line), and the Jefimenko equation for elements only along the line-of-sight, E_{LOS} (dash-dot line), versus observer time t_{obs} for the simplified case where the standard atmosphere is replaced by a constant density air slab and the conduction current is neglected. Each electric field has been normalized so that their peak value is one. Only the Jefimenko solution E_{JEF} has the same time-dependence as the CHAP electric field E_{CHAP}. This comparison shows that the CHAP electric field is not a superposition of signals along the LOS.

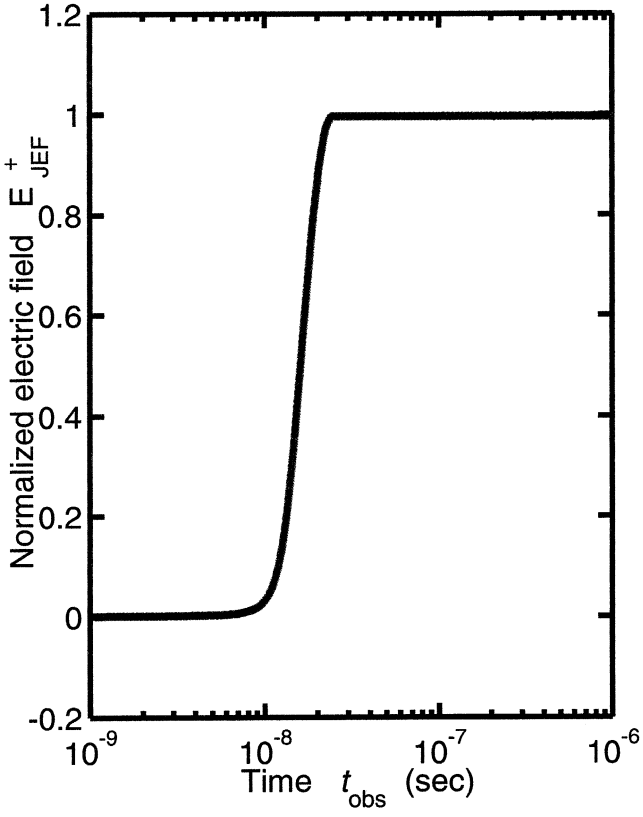

Fig. 6. Normalized electric field E^{+}_{JEF} versus observer time t_{obs} calculated using only the $\dot{J}_C > 0$ part from Fig. 3 as the source in the Jefimenko equation. The long pulse width and flattened top is due to the constant rate of arrival signals of the same sign at the ground observer.

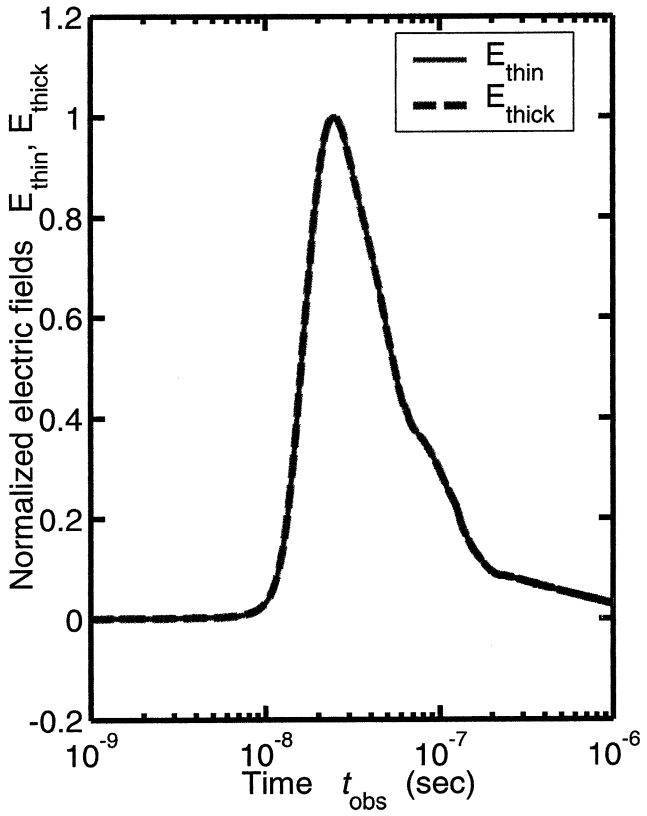

Fig. 7. Comparison of the normalized electric field from a thin shell (solid line) and a thick shell (dashed line) such as E_{CHAP} from Fig. 5 for the simplified case. Both calculations used the Jefimenko equation and the same source $\dot{J}_C$. The thickness of the thin shell is $\Delta r = 0.5\,\mathrm{m}$. The thickness of the thick shell is $\Delta r = 10\,\mathrm{km}$. The overlap of the two curves suggests the spherical curvature of the source is important in establishing the time-dependence of the EMP electric field.

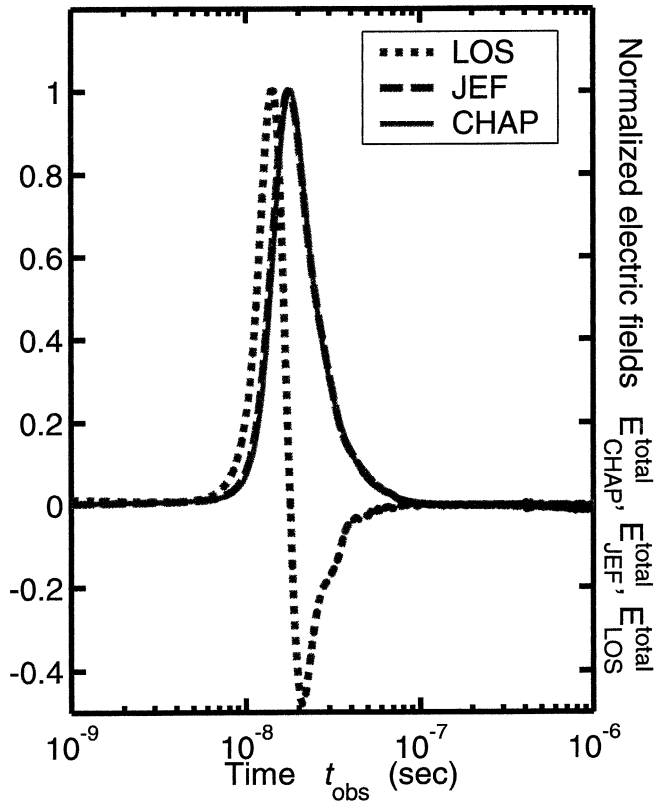

Fig. 8. Comparison of electric fields calculated with CHAP, E_{CHAP} (solid line), the Jefimenko equation, E_{JEF} (dashed line), and the Jefimenko equation applied to elements along the line-of-sight, E_{LOS} (dash-dot line), versus observer time t_{obs} for the standard case. Each curve has been normalized so that their peak value is one. Again, only the Jefimenko solution E_{JEF} has the same time-dependence as the CHAP electric field E_{CHAP}.

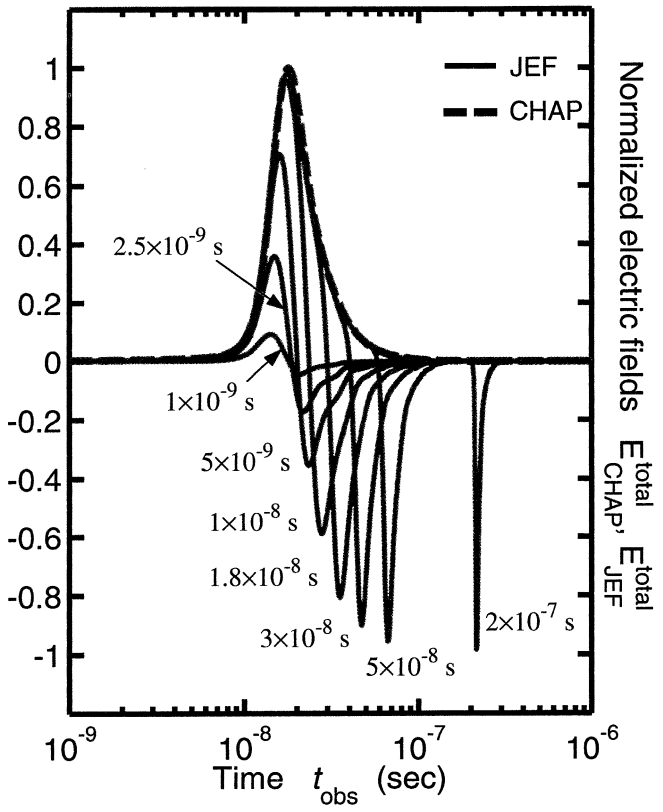

Fig. 9. Comparison of the CHAP electric field E_{CHAP} (dashed line) for the standard case with the electric field from seven different calculations using the Jefimenko equation (solid lines). Each of the solid lines is marked with a number given by $(r+R)/c$ (see Fig. 1) which corresponds to the size of the ellipsoid of causality. As the size numbers increase the size of the source region integrated in the Jefimenko equation also increases. Notice that the solution given by the Jefimenko equation matches the CHAP solution E_{CHAP} as larger sizes are used. The development of the large negative pulse is not real since they occur at times greater than the size number.

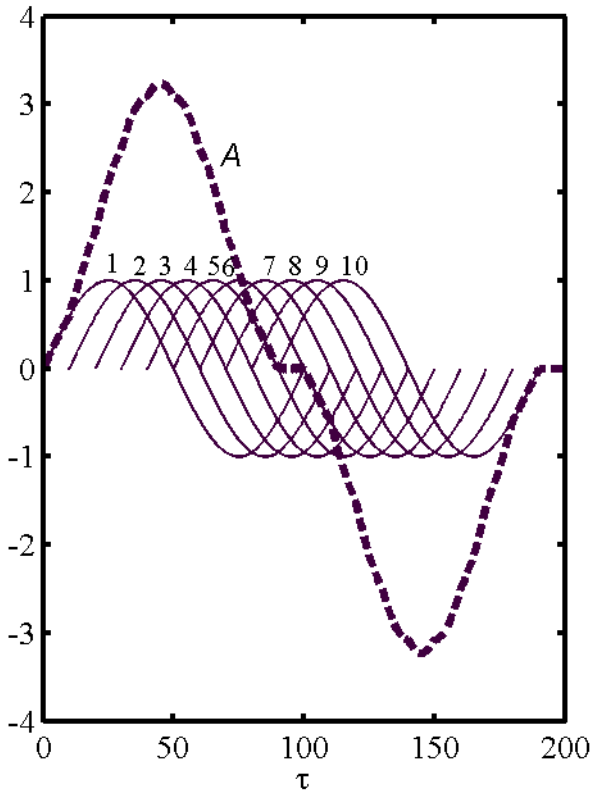

Fig. 10. $A(\tau)$ (dashed line) is the summation of ten single cycle sinusoids (solid lines) that begin at intervals of 1/10 of a period from one another. Notice that the time-dependence of the resultant $A(\tau)$ is not the same as the sinusoids. The curve *A* peaks at the point when the negative part of sinusoid 1 becomes negative. Afterwards the curve *A* decreases due to more negative contributions from the sinusoids. The curve *A* is then zero from τ = 90-100 because of cancellation The time development of the EMP electric field is similar to this toy model except the resultant is the EMP electric field and instead of summing sinusoids we sum signals proportional to $\dot{J}$ with arrival times given by the path length $(r+R)/c$ (see Fig. 1).

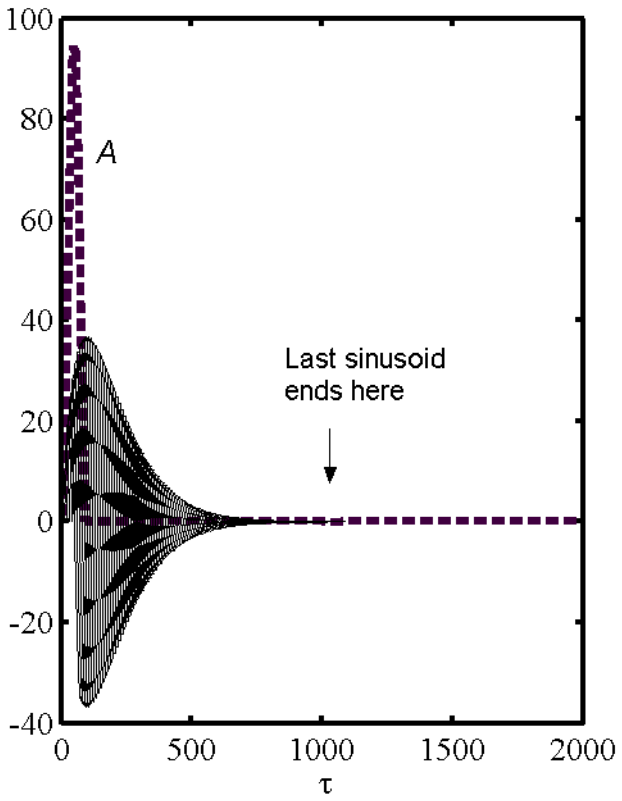

Fig. 11. $A(\tau)$ (dashed line) is the summation of one hundred single cycle sinusoids with amplitude $\tau\exp(-\tau/100)$ that begin at intervals of 1/10 of a period from one another. The late time negative pulse in the curve that showed up in Fig. 10 is not present because the amplitude of the late time sinusoids goes to zero. The decay of the amplitude of the sinusoids is more realistic than the constant amplitude shown in Fig. 10.